AGU ADVANCING EARTH AND SPACE SCIENCE

Geophysical Research Letters

RESEARCH LETTER
10.1029/2020GL088922

Interdecadal Pacific Oscillation Drives Enhanced Greenland Surface Temperature Variability During the Last Glacial Maximum

Zhaoyang Song[1,2], **Mojib Latif**[1,3], **Wonsun Park**[1], **and Yuming Zhang**[4]

[1]GEOMAR Helmholtz Centre for Ocean Research Kiel, Kiel, Germany, [2]School of Atmospheric Sciences, Sun Yat-sen University, Zhuhai, China, [3]Faculty of Mathematics and Natural Sciences, Christian Albrechts University, Kiel, Germany, [4]South China Institute of Environmental Sciences, Ministry of Ecology and Environment of the People's Republic of China, Guangzhou, China

Key Points:
- Oxygen isotope records and climate modeling show large reductions in Greenland surface temperature variability from the LGM to modern times
- Atmospheric teleconnections from the Interdecadal Pacific Oscillation intensify under glacial conditions
- Greenland surface temperature is forced by atmospheric heat transport and sea ice linked to the Interdecadal Pacific Oscillation

Supporting Information:
- Supporting Information S1

Correspondence to:
Y. Zhang,
ymzhang85@126.com

Citation:
Song, Z., Latif, M., Park, W., & Zhang, Y. (2020). Interdecadal Pacific Oscillation drives enhanced Greenland surface temperature variability during the Last Glacial Maximum. *Geophysical Research Letters*, *47*, e2020GL088922. https://doi.org/10.1029/2020GL088922

Received 16 MAY 2020
Accepted 11 NOV 2020
Accepted article online 23 NOV 2020

Abstract Stable oxygen isotope records from central Greenland suggest disproportionally large long-term surface air temperature (SAT) variability during the Last Glacial Maximum (LGM) relative to preindustrial times. Large perturbations in mean atmospheric circulation and its variability forced by extensive Northern Hemisphere ice sheet coverage have been suggested as cause for the enhanced Greenland SAT variability. Here, we assess the factors driving Greenland SAT variability during the LGM by means of dedicated climate model simulations and find remote forcing from the Pacific of critical importance. Atmospheric teleconnections from the Interdecadal Pacific Oscillation (IPO), a multidecadal oscillation of sea surface temperature in the Pacific Ocean, strongly intensify under LGM conditions, driving enhanced surface wind variability over Greenland, which in turn amplifies SAT variability by anomalous atmospheric heat transport. A major role of the IPO in forcing Greenland SAT variability also is supported by a number of models from the Paleoclimate Modeling Intercomparison Project Phase III.

Plain Language Summary Stable oxygen isotope records, a proxy for the local surface air temperature (SAT), from central Greenland indicate disproportionally large reductions in the multidecadal variability from the Last Ice Age (Last Glacial Maximum, LGM; about 21,000 years before present) to modern times. A climate model simulates the changes in multidecadal Greenland SAT variability as inferred from the proxy data. The enhanced variability during the LGM is largely remotely driven by the Interdecadal Pacific Oscillation (IPO), a multidecadal oscillation of sea surface temperature (SST) in the Pacific Ocean. Atmospheric teleconnections from the IPO strongly intensify under glacial conditions, driving enhanced surface wind variability over Greenland and through atmospheric heat transport the SAT variability.

1. Introduction

Local surface air temperature (SAT) variability significantly affects Greenland ice sheet surface mass balance (Hanna et al., 2008, 2011), with impacts on global sea level through freshwater runoff (Bindoff et al., 2007; Lemke et al., 2007), and climate through altered ocean circulation (Fichefet et al., 2003; Rahmstrof et al., 2005). Stable oxygen isotope ($\delta^{18}O$) records from central Greenland ice cores, providing high-resolution SAT reconstructions (Andersen et al., 2004; Masson-Delmotte et al., 2005), suggest enhanced SAT variability linked to more variable atmospheric circulation during the last glacial relative to the last millennium (Ditlevsen et al., 1996; Shao & Ditlevsen, 2016). Along with lower atmospheric greenhouse gas concentrations, excessive Northern Hemisphere continental ice sheet coverage has been recognized as an important forcing of large perturbations in atmospheric circulation (e.g., Hofer et al., 2012; Justino & Peltier, 2005; Pausata et al., 2009, 2011), with colder sea surface temperature (SST) and larger sea ice extent as additional possible drivers of the atmospheric circulation (Byrkjedal et al., 2006; Kageyama et al., 1999). Marine and terrestrial temperature proxies around the globe reveal that the variability over Greenland went through disproportionally strong weakening from the Last Glacial Maximum (LGM) to the present as compared to other regions (Rehfeld et al., 2018). For instance, the multicentennial to millennial Greenland SAT variability decreased by a factor of 73 from the LGM to the Holocene, as compared to mild reductions by only

a factor of 1.6–2.8 in the tropics and 8.0–14.0 in the northern mid-latitudes (Rehfeld et al., 2018). In this study, we investigate the origin of the disproportionally strong change in the SAT variability over Greenland.

The North Atlantic Oscillation (NAO), the leading mode of atmospheric variability over the North Atlantic, is known to affect Southern Greenland SAT by shifting the position of the jet stream and storm track (Andres & Peltier, 2013; Hanna et al., 2013; Hurrell, 1995; Hurrell et al., 2003). Greenland surface mass balance reconstruction for the period of 1870–2010 exhibits statistically significant correlation with the NAO (Hanna et al., 2008). The Atlantic Multidecadal Oscillation (AMO) also termed Atlantic Multidecadal Variability (AMV), a spatially coherent pattern of SST variability over the North Atlantic with a period of 60–80 years, influences southern Greenland SAT by modulating the NAO and Greenland Sea ice cover (Grossmann & Klotzbach, 2009; Kobashi et al., 2015; Rimbu et al., 2017). However, the mechanisms by which the atmosphere, specifically the NAO, responds to extratropical SST anomalies are still highly controversial. Stand-alone atmosphere model experiments qualitatively demonstrated that atmospheric variability is more affected by local internal atmospheric processes than by the extratropical SST anomalies under glacial and present-day conditions (Kushnir et al., 2002; Pausata et al., 2009). Sea ice anomalies also can potentially affect the phase and amplitude of the NAO (Deser et al., 2000; Seierstad & Bader, 2009).

Over the Pacific El Niño–Southern Oscillation (ENSO)-like multidecadal SST variations exist, referred to as the Interdecadal Pacific Oscillation (IPO) (Deser et al., 2004; Liu, 2012; Zhang et al., 1997). It has been shown that the IPO influences the NAO through atmospheric teleconnections on multidecadal timescales (Latif, 2001; Parker et al., 2007) and thus Southern Greenland SAT (Dong & Dai, 2015). Yet little attention has been payed so far to this teleconnection when discussing the pronounced weakening of Greenland-SAT variability from the LGM to the present. Here we investigate the role of the IPO in the weakening of the variability by conducting a set of climate model experiments under LGM and preindustrial conditions.

2. Methods and Experimental Setup

In order to obtain insight into the mechanisms underlying the change in variability, simulations are performed with the Kiel Climate Model (KCM; Park et al., 2009). The KCM is a fully coupled atmosphere-ocean-sea ice general circulation model, which consists of the atmosphere model ECHAM5 (Roeckner et al., 2003) and the ocean-sea ice model NEMO (Madec, 2008). In the version applied here, the atmospheric component ECHAM5 is used with a horizontal resolution of T42 (2.8° × 2.8°) and 19 vertical levels reaching up to 10 hPa. In ECHAM5, land surface temperature is calculated through the energy balance. An implicit coupling scheme between the land and the atmosphere is used (Schulz et al., 2001), which is unconditionally stable and allows for synchronous surface flux calculations. NEMO consists of OPA for the ocean dynamics and thermodynamics and LIM for the sea ice dynamics and thermodynamics. The horizontal resolution of NEMO is approximately 2° (ORCA2 grid), with a meridional refinement of ~0.5° near the equator and 31 vertical levels. The two models are coupled with the OASIS3 coupler (Valcke, 2006).

Two simulations are performed: a 5,300-year-long preindustrial control run (PI) that is initialized with the Levitus temperature and salinity climatology. The Levitus data set provides long-term means of objectively analyzed ocean temperature and salinity at multiple depths (Conkright et al., 1998). The PI simulation employs preindustrial CO_2 concentration (286 ppm), modern land-sea mask, orography, and continental ice sheet configuration. In the other 5,600-year-long simulation (LGM), the boundary conditions, greenhouse gas concentrations, and orbital parameters are implemented in accordance with the Paleoclimate Modeling Intercomparison Project Phase 4 (PMIP4) protocol for LGM experiments (Kageyama et al., 2017). The ice sheet configuration is an average of three different reconstructions following the Paleoclimate Modelling Intercomparison Project Phase III (PMIP3) LGM experiments (Braconnot et al., 2012). To account for the 116-m drop of the mean sea level, the LGM simulation is initialized with Levitus temperature climatology and salinity climatology to which 1 psu has been added. The simulated mean climate and multidecadal Atlantic Meridional Overturning Circulation (AMOC) variability has been addressed in detail in a previous study (Song et al., 2019). The output of the last 1,000 years of the two simulations is analyzed, and 5-year mean anomalies are computed in this study. To calculate 5-year mean anomalies, monthly

anomalies are calculated first and then averaged into 5-year bins. This yields a total number of 200 5-year mean anomalies.

2.1. Restoring Experiments

To support the results from the fully coupled model, partially coupled experiments are performed, in which SST over the Pacific (50°S–45°N, 140°E–90°W) is restored to climatology, hereafter referred to as PI_{res} and LGM_{res}. The SSTs in the PI_{res} and LGM_{res} simulations are restored over the nudging region to monthly SST climatology calculated from the PI and LGM experiments, respectively, and with a relaxation timescale of 30 days (supporting information Figure S1). The restoring largely eliminates the SST variability over the Pacific including the IPO. Each experiment is integrated for 600 years, with the monthly output taken for analysis. Two additional partially coupled experiments are performed that are referred to as PI_{resTP} and LGM_{resTP}. The setup in these simulations is the same as in the PI_{res} and LGM_{res} experiments, except that in the PI_{resTP} and LGM_{resTP} simulations only the SSTs over the tropical Pacific (20°S–20°N, 140°E–90°W) are restored.

2.2. Stand-Alone Atmosphere Model Experiments

Two sets of stand-alone atmosphere model experiments, each set consisting of four integrations, are conducted with ECHAM5, in order to investigate the sole influence of either IPO-related SST anomalies over the Pacific or IPO-related sea ice concentration (SIC) anomalies over the North Atlantic and Arctic on Greenland SAT. Both the composite anomalies of the positive IPO and negative IPO polarity are used to force the atmosphere model. In the first set of stand-alone atmosphere model experiments (Table S1), the IPO-SST composite anomalies (supporting information Figure S2) are used as forcing and ECHAM5 is integrated under the PI and LGM conditions. SIC is set to the respective climatology. The second set (Table S2) is identical to the first but now IPO-SIC composite anomalies drive ECHAM5 (supporting information Figure S3), whereas SST is set to climatology. Each atmosphere model experiment is integrated for 60 years. Monthly output from the last 50 years is taken for analysis.

2.3. Tripole IPO Index

To quantify the IPO variability, a tripole SST index (TPI) is used (Henley et al., 2015). First, monthly SST anomalies averaged over each of the three TPI regions are calculated (black boxes in Figure 2a). The IPO index is defined as the difference between the SST anomalies over the central equatorial Pacific and the average of the SST anomalies over the northwest and southwest Pacific (boxes in Figure 2a). Consistent with the processing of the $\delta^{18}O$ records, we calculate from the model an IPO index that is based on 5-year means. SST and SIC composites are computed using the periods when the IPO index exceeds a threshold of ± 1 standard deviation.

2.4. Niño3.4 Index

In order to distinguish IPO-related SST variability from that linked to the ENSO, which is the leading mode of interannual SST variability in the tropical Pacific, we use the so-called Niño3.4 index. This index represents the equatorial Pacific SST anomalies averaged over the region 5°N–5°S and 170°W–120°W.

2.5. Eliassen-Palm Flux

To diagnose the meridional eddy fluxes of heat and zonal momentum associated with the IPO over the Atlantic sector (70°W–15°W), the Eliassen-Palm flux (E-P flux; Edmon et al., 1980) and its divergence in the quasi-geostrophic approximation is calculated as

$$F^{(\varphi)} = -a\cos\phi\overline{u'v'}$$

$$F^{(p)} = a\cos\phi f\frac{\overline{v'\theta'}}{\overline{\theta}_p}$$

$$\nabla\cdot\boldsymbol{F} = \frac{\partial F^{(\varphi)}}{\partial a\cos\phi} + \frac{\partial F^{(p)}}{\partial p}$$

where a is the radius of the Earth, f the Coriolis parameter, ϕ is the latitude, θ the potential temperature, p the pressure, and (u, v) the zonal and meridional wind. Subscripts denote partial derivatives, and eddies

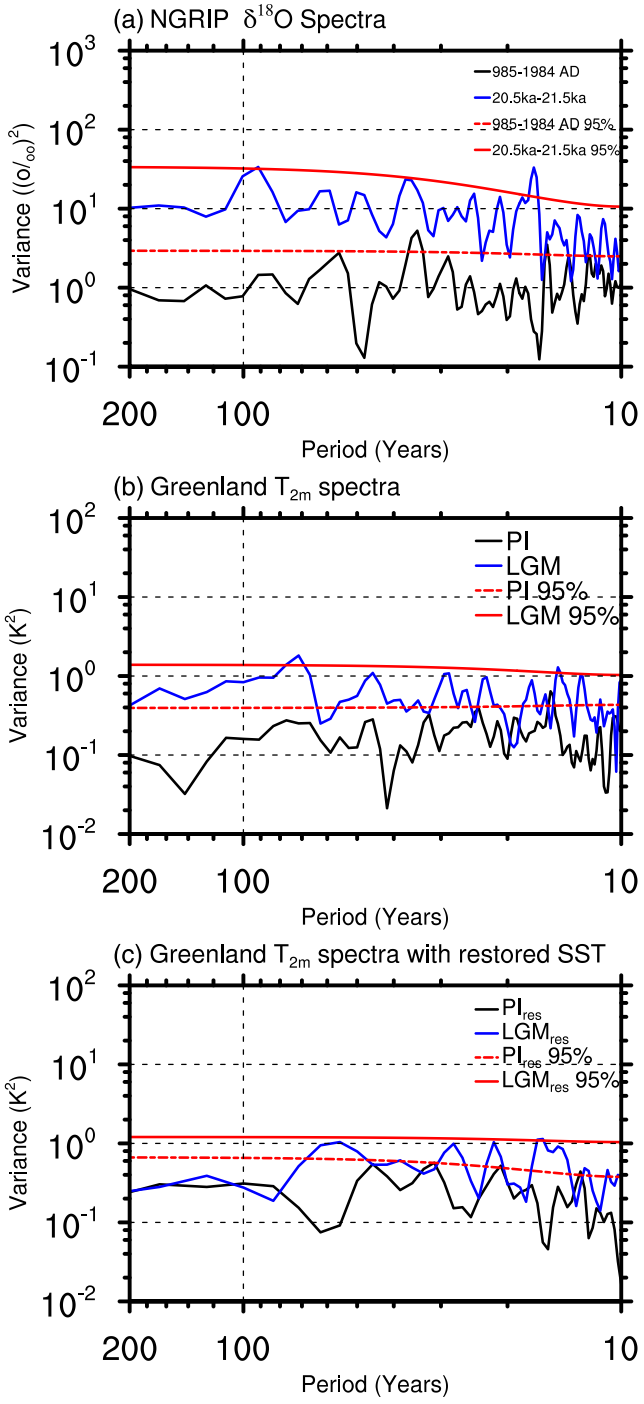

Figure 1. (a) Spectra of 5-year mean $\delta^{18}O$ ratio (per million) from the Northern Greenland Ice Core Project (NGRIP) during the last millennium (985–1984) and LGM (21.5–20.5 kyr before present). The red dashed and solid lines indicate the 95% confidence limit of the Markov Red Noise model for the last millennium and LGM, respectively. (b) As in (a) but for SAT averaged over Greenland in the PI and LGM simulations. (c) As in (a) but for SAT averaged over Greenland in the restoring experiments PI_{res} and LGM_{res}.

(primed quantities) are calculated with respect to the zonal mean. All eddy quantities are calculated from 1,000-year daily output and then averaged over 5 years. $F^{(\varphi)}$ is the meridional flux of zonal momentum, and $F^{(p)}$ is the meridional heat flux by the eddies. The positive (negative) E-P flux divergence represents an acceleration (a deceleration) of the westerly mean zonal flow.

For a graphical display in latitude-pressure coordinates, $F^{(\varphi)}$ and $F^{(p)}$ are scaled as follows

$$\left\{\widetilde{F}_{\varphi}, \widetilde{F}_{p}\right\} = \cos\phi \times \left\{\frac{{}^{1}/_{a}F^{(\varphi)}}{s_{\varnothing}}, \frac{F^{(p)}}{s_{p}}\right\}$$

where $s_{\varnothing}$ equals to π radians and s_p is 10^5 Pa.

3. Results

We first analyze the Northern Greenland Ice Core Project (NGRIP) $\delta^{18}O$ data from central Greenland (75.10°N, 42.32°W; supporting information Figure S4a), which provide estimates of seasonal-to-millennial Greenland SAT variations. To highlight the multidecadal variability, we calculate 5-year mean values from the raw data (supporting information Figure S4b). We consider two 1,000-year long epochs, 21.5–20.5 kyr before present (LGM) and the last millennium (985–1984). Clearly, the variability during the last millennium (supporting information Figure S4c) is much weaker than that in the LGM (supporting information Figure S4d), which can be readily seen in the spectra (Figure 1a).

3.1. Coherent Multidecadal Variations of IPO and Greenland SAT

The spectrum of the 5-year mean SAT anomalies averaged over Greenland exhibits enhanced multidecadal variability in the LGM relative to the PI simulation (Figure 1b), illustrating some consistency of the model simulations with the proxy data (Figure 1a). However, there are noticeable differences, which reflect model bias, and/or biased or incomplete forcing (Kajtar et al., 2019; Power et al., 2017). Yet we conclude that the model reproduces the salient feature in the change of SAT-variability over Greenland.

The 5-year mean anomalies are regressed on the 5-year mean Greenland SAT (unit: K). In PI, variability of Greenland SAT is mostly linked to local processes, that is, variations in the atmospheric circulation, over the North Atlantic (Figure 2a), consistent with National Centers for Environmental Prediction/Climate Forecast System Reanalysis (Saha et al., 2010) and ERA-Interim (Dee et al., 2011) reanalyses (supporting information Figure S5). In the LGM simulation, on the other hand, the regression pattern suggests processes over the North Atlantic and tropical Pacific drive SAT variability over Greenland (Figure 2b). The regression pattern over the Pacific in the LGM experiment resembles the IPO pattern with centers of action over the equatorial and northwest and southcentral Pacific. In contrast to the PI simulation, the regression coefficients in the LGM simulation are statistically significant over large parts of the Pacific.

Cross-spectral analysis is applied to evaluate in frequency domain the relationship between Greenland SAT and the IPO index. High squared coherence is consistently observed at decadal to centennial timescales in

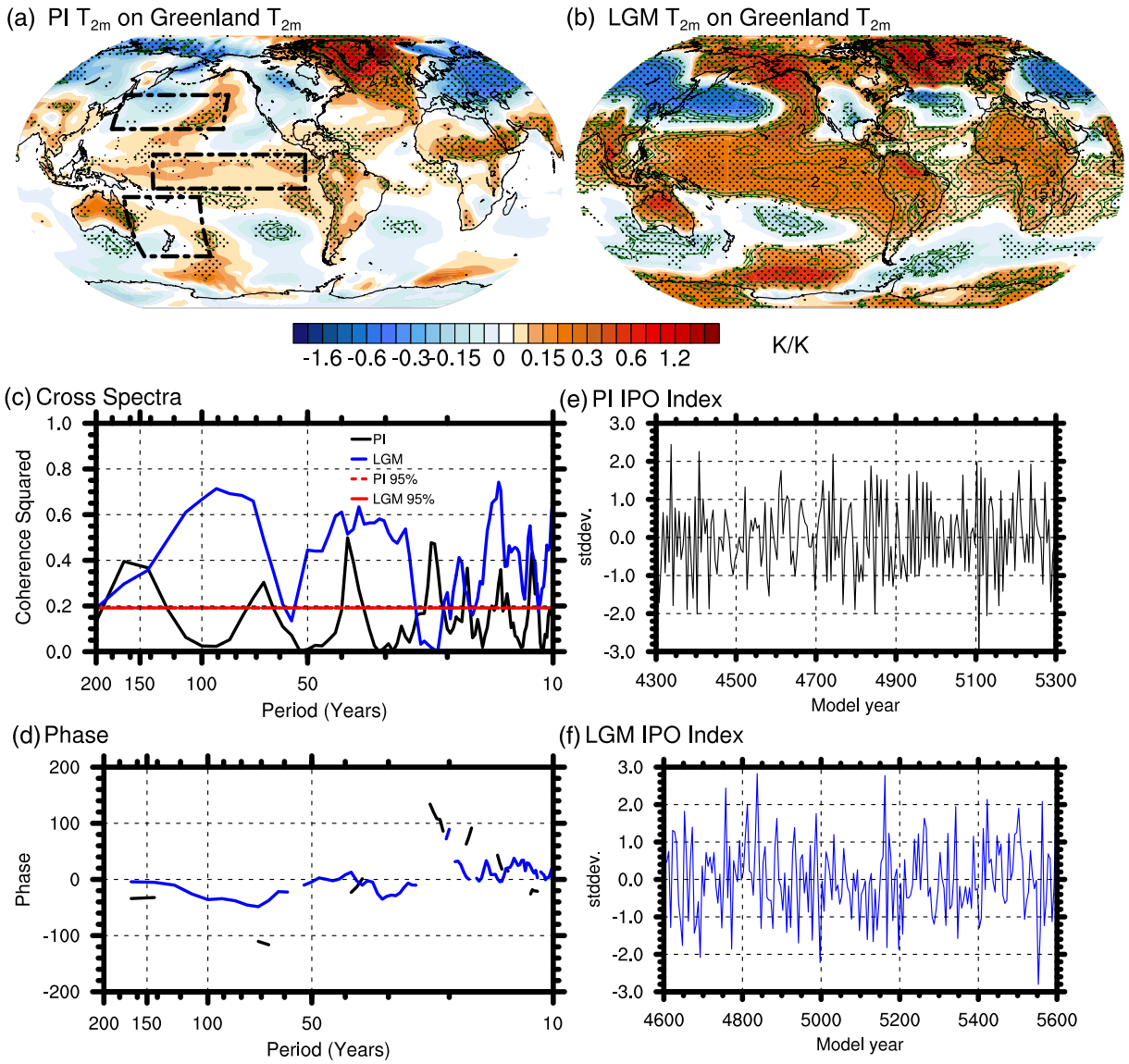

Figure 2. Regressions (K/K) of 5-year mean SAT anomalies on the 5-year mean SAT averaged over Greenland for the (a) PI and (b) LGM simulations. Stippling indicates significance at the 95% confidence interval using *p* value test. (c, d) Results from cross-spectral analysis between the tripole IPO index and Greenland SAT. (c) Squared coherence spectrum of the IPO index and Greenland SAT in the PI and LGM experiments. The red dashed and solid lines indicate the 95% confidence limit for the squared coherence. (d) Phase spectrum between the IPO index and Greenland SAT. Positive phase refers to the IPO index leading the variations in Greenland SAT. Note that phase only is shown at frequencies with statistically significant squared coherence. 5-year mean IPO index in the (e) PI (black) and (f) LGM (blue).

the LGM but not in the PI (Figure 2c). Phase estimates indicate that the IPO index is generally in phase with or slightly leads (positive phases) the variations of Greenland SAT at periods of up to 50 years (Figure 2d), supporting the notion of remote forcing by the Pacific. On longer timescales, the IPO index lags Greenland SAT anomalies by approximately one decade, which possibly could be related to interactions between the AMOC, AMV, and IPO through the Walker Circulation (Levine et al., 2017).

3.2. Climatic Response to IPO Forcing

Selected variables are regressed over the North Atlantic sector on the IPO index. During the positive phase of the IPO, geopotential height anomalies at 250 hPa in the PI and LGM simulations exhibit a dipole structure with decreased meridional gradient over the middle- to high-latitude North Atlantic (Figures 3a and 3b). The IPO-related atmospheric circulation change over the North Atlantic is equivalent barotropic in the two

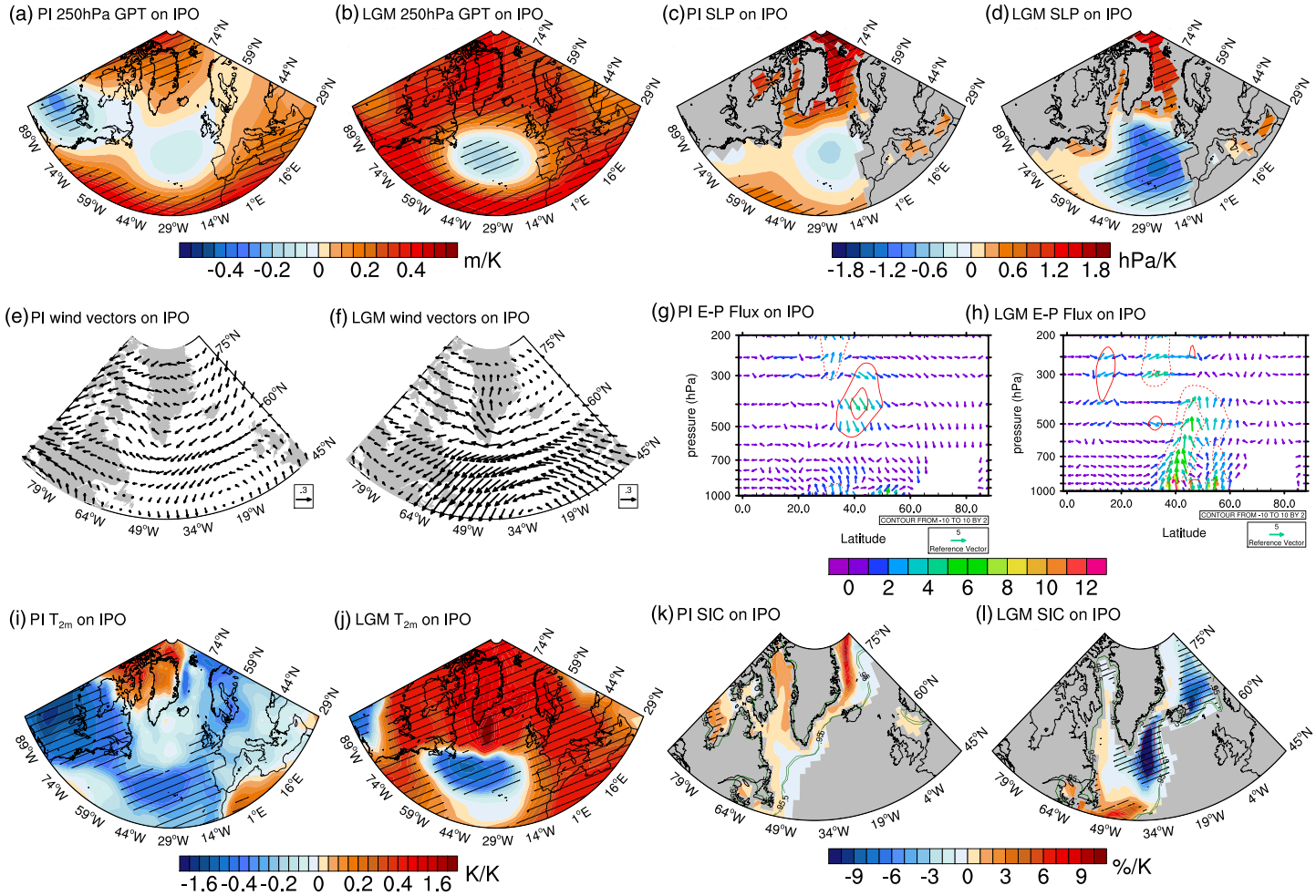

Figure 3. Regressions of selected quantities on the 5-year mean IPO index. Regressions (m/K) of geopotential height (GPT) anomalies at 250 hPa in the (a) PI and (b) LGM simulations. Regressions (hPa/K) of sea level pressure (SLP) anomalies in the (c) PI and (d) LGM. Regressions (m/s/K) of wind anomalies at 700 hPa in the (e) PI and (f) LGM. Regressions of Eliassen-Palm flux (E-P flux, vectors) over the Atlantic sector (70°W–15°W) and its divergence (contours) in the (g) PI and (h) LGM. Dashed (solid) red contours indicate the convergence (divergence) of E-P flux, which represents a deceleration (an acceleration) of the westerly mean zonal flow. Missing values indicate the elevation and location of the Greenland ice sheet in the model. Regressions (K/K) of SAT anomalies in the (i) PI and (j) LGM. Regressions (%/K) of sea ice concentration (SIC) anomalies in the (k) PI and (l) LGM. The green contours indicate the range for 95% sea ice concentration. Red contours (contour interval: 10%) indicate the variance explained by the IPO index. Hatching indicates significance at the 95% confidence interval using *p* value test.

simulations (Figures 3c and 3d). However, the magnitude of the height anomalies is much larger in the LGM (~0.40 m) relative to the PI (~0.15 m). Only in the LGM experiment are both centers of action statistically significant. Southeasterly wind anomalies are implied over large parts of Greenland by the circulation change, which are much stronger in the LGM relative to the PI, as shown by the wind anomalies at the 700-hPa level (Figures 3e and 3f). We note a statistically significant negative anomaly over North America in the PI that is missing in the LGM.

To estimate the changes in the atmospheric eddy fluxes of momentum and heat, the E-P flux and its divergence are calculated and regressed on the IPO index. Negative E-P flux divergence (dashed contours in Figures 3g and 3h) over 30°N–60°N supports stronger westerly zonal wind anomalies over the North Atlantic in LGM (Figures 3e and 3f). During the positive phase of the IPO, large upward E-P flux vectors indicate much enhanced northward heat transport by eddies over the Atlantic sector (70°W–15°W) north of 35°N in the LGM experiment (Figures 3g and 3h). Additionally, the wave-activity flux (supporting information Text), a measure for the momentum flux by the quasi-stationary Rossby waves on the zonally varying westerlies (Takaya et al., 2001), confirms that the atmospheric teleconnections associated with the IPO is

stronger in the LGM relative to the PI (supporting information Figure S6). Thus, the forcing of Greenland SAT by the IPO is considerably amplified in the LGM (Figures 3i and 3j).

Reduced SIC southeast of Greenland (Figure 3l) also would lead to warming over Greenland in LGM (Drijfhout et al., 2013; Kleppin et al., 2015; Rhines & Huybers, 2014). When regressed on the IPO index, statistically significant SIC changes are absent around Greenland in the PI experiment (Figure 3k). The IPO index in the LGM simulation, however, accounts for up to 20% of total SIC variance over the Irminger Sea and south of Greenland (red contours in Figure 3l), suggesting a potential SIC impact on Greenland SAT. We note that during the satellite era, links between Greenland sea ice concentration and SST to Greenland SAT extremes and related Greenland ice sheet surface mass balance changes also have been documented (e.g., Ballinger et al., 2018; Noël et al., 2014).

We performed two partially coupled experiments, termed PI_{res} and LGM_{res}, which are identical to the PI and LGM simulations except that SST is restored to climatology over the tropical and mid-latitude Pacific (supporting information Figure S1). The SST variability is essentially eliminated over the restoring domain, including the IPO and its teleconnections. The multidecadal variability of Greenland SAT in the LGM_{res} simulation considerably weakens relative to the fully coupled experiment LGM (Figure 1b) and is of similar magnitude as in the PI simulation (Figure 1c). This confirms the important role of the IPO in driving Greenland SAT in LGM in our model.

3.3. Relative Importance of Atmospheric Teleconnections and Sea Ice for Greenland SAT Variability

Enhanced multidecadal Greenland SAT variability in the LGM relative to the PI is attributed to stronger IPO-related atmospheric teleconnections as well as sea-ice influence. We performed two sets of stand-alone atmosphere model experiments (supporting information Figures S2 and S3), in order to investigate the relative roles of the two factors. In the first set consisting of four experiments (Table S1), the atmosphere model is forced over the Pacific by composite SST anomalies calculated for negative and positive IPO phases, and the experiments are performed under PI and LGM conditions. SIC is set to the respective climatology. This set yields insight into the impact of atmospheric teleconnections from the Pacific on Greenland SAT. The results are shown in terms of the SAT response difference between the experiments employing positive and negative composite SST anomalies ($PI_{SST+} - PI_{SST-}$ and $LGM_{SST+} - LGM_{SST-}$). There is no statistically significant temperature signal over Greenland when the atmosphere model is integrated under PI conditions (Figure 4a). In contrast, a statistically significant warming signal is observed over Greenland under LGM conditions (Figure 4b). The marked difference between the stand-alone experiments performed under PI (Figure 4a) and LGM (Figure 4b) conditions is linked to the 700-hPa wind responses. Strong changes in the zonal and meridional winds over south and central Greenland only exist under LGM conditions, whereas wind signals under PI conditions are considerably smaller (supporting information Figures S7a and S7b).

The second set of stand-alone experiments (Table S2) explores the influence of IPO-related SIC variations. This set is analogous to the first set but instead of composite SST anomalies, composite SIC anomalies drive the atmosphere model and SST is set to climatology. Again, the signal is rather weak under PI conditions (Figure 4c), whereas it is much stronger under LGM conditions (Figure 4d). This again can traced back to the 700-hPa wind response that is much stronger under LGM conditions (supporting information Figures S7c and S7d). The stand-alone atmosphere model experiments also support an important role of the IPO for Greenland SAT variability under LGM conditions, and they reveal that it is mostly the IPO-related teleconnections from the Pacific and to a lesser extent the IPO-related SIC changes driving Greenland SAT variability.

We also investigate the link of Greenland SAT to the IPO in eight models participating in the PMIP3 (supporting information Table S3), which provide output for the PI and LGM setups. The correlation between the 5-year mean IPO index and 5-year mean Greenland SAT is calculated. Consistent with the KCM results, three out of the eight PMIP3 models exhibit a significantly larger correlation in the LGM relative to the PI, that is, a stronger link of the Greenland SAT to the IPO in the LGM (supporting information Figure S8).

The IPO-related SST anomalies exhibit a similar spatial pattern as that linked to the ENSO. Whether the IPO is distinct from ENSO, either physically or statistically, has been debated in many studies (e.g., Dong &

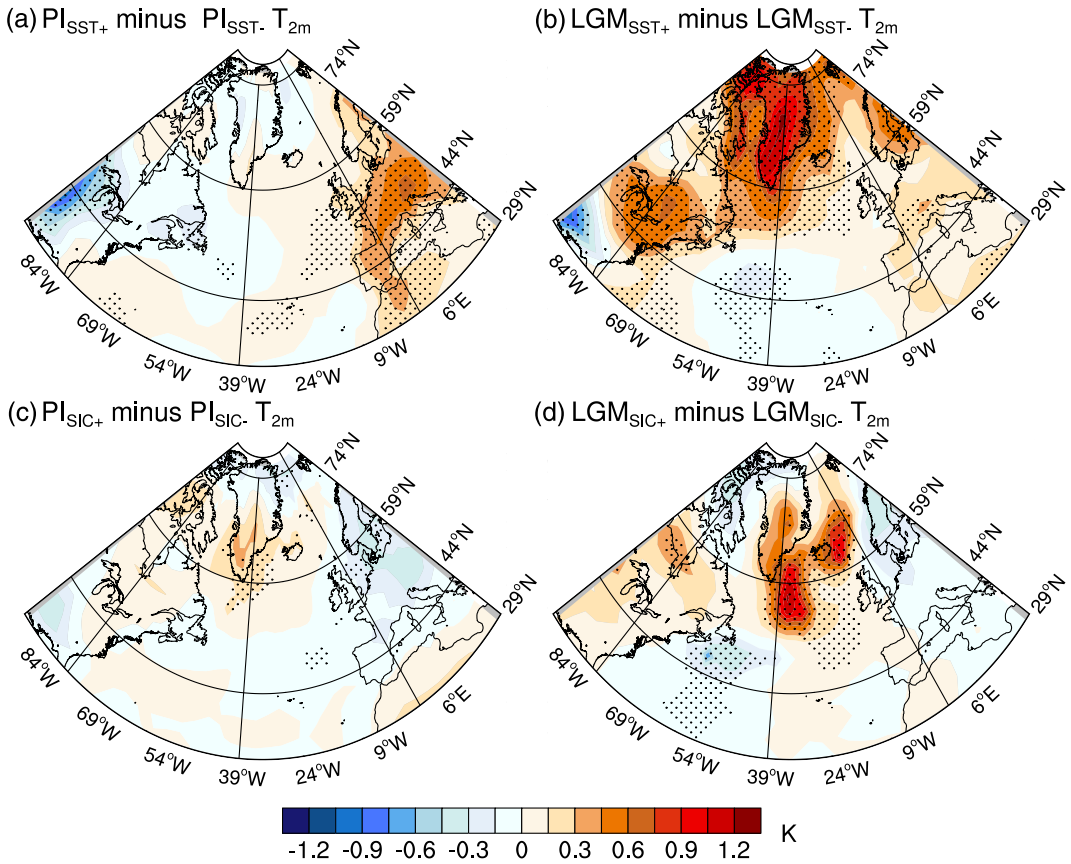

Figure 4. Responses of SAT (unit: K) to the anomalous SST associated with the IPO (positive phase minus negative phase) for the (a) PI and (b) LGM simulations. Responses of SAT (unit: K) to the anomalous sea ice concentration associated with the IPO (positive phase minus negative phase) for the (c) PI and (d) LGM simulations. Stippling indicates the differences are significant at the 95% confidence level using Student's *t* test.

Dai, 2015; Newman et al., 2016). Nevertheless, interannual to decadal ENSO variability can be communicated to the mid-latitude Pacific via the atmospheric bridge (Newman et al., 2016), which by themselves may force Greenland SAT variations. Therefore, we examine the relationship between the ENSO and Greenland SAT. The spectra of the annual-mean Niño3.4 index and Greenland SAT are calculated in the PI and LGM simulations (supporting information Figure S9). The ENSO variability in the LGM is weaker than that in the PI. The variance of 10-year high-pass filtered annual-mean Nino3.4 index amounts to 0.47 and 0.27 K^2 in the PI and LGM simulations, respectively. In contrast, the Greenland SAT variability in the LGM is still considerably stronger than in the PI. The variance of 10-year high-pass filtered annual-mean Greenland SAT is 0.24 and 0.53 K^2 in the PI and LGM simulations.

Two additional partially coupled experiments are performed, PI_{resTP} and LGM_{resTP}, in which only the SSTs over the tropical Pacific (20°S–20°N, 140°E–90°W) are restored (supporting information Figure S10). Despite that the ENSO variability is essentially eliminated, the variability of the Greenland SAT remains stronger in the LGM_{resTP} simulation in comparison to the PI_{resTP} simulation (supporting information Figure S11). This supports the notion that it is the extratropical variability associated with the IPO that in our model primarily forces the Greenland SAT rather than its tropical part and thus ENSO.

4. Summary and Discussion

Proxy data suggest an enhanced multidecadal Greenland SAT variability during the LGM relative to the present. Based on simulations with the KCM and models participating in the PMIP3, we propose that the enhanced multidecadal Greenland SAT variability can be largely attributed to the IPO, a mode of

low-frequency SST variability over the Pacific, which drives global atmospheric teleconnections that also changes the atmospheric circulation over the North Atlantic and Northern Hemisphere sea ice. Both the atmospheric teleconnections and the sea ice variability intensify under LGM conditions, thereby enhancing lower-atmosphere wind variability over the North Atlantic/Greenland sector and in turn Greenland-SAT variability through increased atmospheric eddy heat transport. In our model, the teleconnections from the IPO better explain the enhanced multidecadal Greenland-SAT variability in the LGM compared to the forcing from ENSO and SIC. Moreover, partially coupled experiments with the model reveal that it is the extratropical SST variability associated with the IPO that primarily gives rise to the enhancement of the multidecadal Greenland SAT variability during the LGM.

However, the changes in the atmospheric teleconnections under different background climatic states remains controversial, thus deserving further research (e.g., Hu et al., 2020; Merkel et al., 2010). Further, the atmospheric response to extratropical SST anomalies also is under debate. This study suggests that atmospheric teleconnections from the Pacific can strongly change under different external forcing and boundary conditions, and thus under different climatic background states. This could be of importance in the interpretation of proxy data from different regions of the globe. Finally, we suggest longer output from future PMIP simulations, as the current PMIP3 output, which is limited to 100 years, is inadequate to assess multidecadal climate variability and its drivers.

Data Availability Statement

The $\delta^{18}O$ estimates from the North Greenland Ice Core Project are available from the Centre for Ice and Climate at the Niels Bohr Institute, University of Copenhagen via the link (http://www.iceandclimate.nbi.ku.dk/data/). Output from the KCM simulations presented in this study is available at the Pangaea repository (https://doi.pangaea.de/10.1594/PANGAEA.922864). The PMIP3 data output is available at the website (https://esgf-data.dkrz.de/search/cmip5-dkrz/).

Acknowledgments
We thank Stefan Hagemann and Christian Stepanek for their assistance with setting up the simulations. The integrations with the Kiel Climate Model (KCM) were conducted at the Computing Center of Kiel University (CAU). This is a contribution to the PalMod project funded by the German Federal Ministry of Education and Research.

References

Andersen, K., Azuma, N., Barnola, J. M., Bigler, M., Biscaye, P., Caillon, N., et al. (2004). High-resolution record of Northern Hemisphere climate extending into the last interglacial period. *Nature*, *431*(7005), 147–151. https://doi.org/10.1038/nature02805

Andres, H. J., & Peltier, W. R. (2013). Examining internal and external contributors to Greenland climate variability using CCSM3. *Journal of Climate*, *26*(24), 9745–9773. https://doi.org/10.1175/JCLI-D-12-00845.1

Ballinger, T. J., Hanna, E., Hall, R. J., Miller, J., Ribergaard, M. H., & Høyer, J. L. (2018). Greenland coastal air temperatures linked to Baffin Bay and Greenland Sea ice conditions during autumn through regional blocking patterns. *Climate Dynamics*, *50*(1–2), 83–100. https://doi.org/10.1007/s00382-017-3583-3

Bindoff, N. L., Willebrand, J., Artale, V., Cazenave, A., Gregory, J. M., Gulev, S., et al. (2007). Observations: Oceanic climate change and sea level. In S. Solomon, et al. (Eds.), *Climate Change 2007: The Physical Science Basis. Contribution of Working Group I to the Fourth Assessment Report of the Intergovernmental Panel on Climate Change* (pp. 385–428). Cambridge, UK: Cambridge Univ. Press.

Braconnot, P., Harrison, S. P., Kageyama, M., Bartlein, P. J., Masson-Delmotte, V., Abe-Ouchi, A., et al. (2012). Evaluation of climate models using palaeoclimatic data. *Nature Climate Change*, *2*(6), 417–424. https://doi.org/10.1038/nclimate1456

Byrkjedal, O., Kvamsto, N., Meland, M., & Jansen, E. (2006). Sensitivity of last glacial maximum climate to sea ice conditions in the Nordic Seas. *Climate Dynamics*, *26*(5), 473–487. https://doi.org/10.1007/s00382-005-0096-2

Conkright, M. E., Levitus, S., O'Brien, T., Boyer, T. P., Stephens, C., Johnson, D., et al. (1998). *World Ocean Database 1998 Documentation and Quality Control*. Silver Spring, MD: National Oceanographic Data Center.

Dee, D. P., Uppala, S. M., Simmons, A. J., Berrisford, P., Poli, P., Kobayashi, S., et al. (2011). The ERA-Interim reanalysis: Configuration and performance of the data assimilation system. *Quarterly Journal of the Royal Meteorological Society*, *137*(656), 553–597. https://doi.org/10.1002/qj.828

Deser, C., Phillips, A. S., & Hurrell, J. W. (2004). Pacific interdecadal climate variability: Linkages between the tropics and the North Pacific during boreal winter since 1900. *Journal of Climate*, *17*(16), 3109–3124. https://doi.org/10.1175/1520-0442(2004)017<3109:PICVLB>2.0.CO;2

Deser, C., Walsh, J. E., & Timlin, M. S. (2000). Arctic sea ice variability in the context of recent atmospheric circulation trends. *Journal of Climate*, *13*, 617–633. https://doi.org/10.1175/1520-0442(2000)013<0617:ASIVIT>2.0.CO;2

Ditlevsen, P. D., Svensmark, H., & Johnsen, S. E. (1996). Contrasting atmospheric and climate dynamics of the last-glacial and Holocene periods. *Nature*, *379*, 810–812.

Dong, B., & Dai, A. (2015). The influence of the interdecadal Pacific oscillation on temperature and precipitation over the globe. *Climate Dynamics*, *45*(9–10), 2667–2681. https://doi.org/10.1007/s00382-015-2500-x

Drijfhout, S., Gleeson, E., Dijkstra, H. A., & Livina, V. (2013). Spontaneous abrupt climate change due to an atmospheric blocking–sea-ice–ocean feedback in an unforced climate model simulation. *Proceedings of the National Academy of Sciences*, *110*(49), 19,713–19,718. https://doi.org/10.1073/PNAS.1304912110

Edmon, H. J., Hoskins, B. J., & McIntyre, M. E. (1980). Eliassen-Palm cross sections for the troposphere. *Journal of the Atmospheric Sciences*, *37*, 2600–2616. https://doi.org/10.1175/1520-0469(1980)037<2600:EPCSFT>2.0.CO;2

Fichefet, T., Poncin, C., Goosse, H., Huybrechts, P., Janssens, I., & Le Treut, H. (2003). Implications of changes in freshwater flux from the Greenland ice sheet for the climate of the 21st century. *Geophysical Research Letters*, *30*(17), 1911. https://doi.org/10.1029/2003GL017826

Grossmann, I., & Klotzbach, P. J. (2009). A review of North Atlantic modes of natural variability and their driving mechanisms. *Journal of Geophysical Research*, *114*, D24107. https://doi.org/10.1029/2009JD012728

Hanna, E., Huybrechts, P., Cappelen, J., Steffen, K., Bales, R. C., Burgess, E., et al. (2011). Greenland ice sheet surface mass balance 1870 to 2010 based on twentieth century reanalysis, and links with global climate forcing. *Journal of Geophysical Research*, *116*, D24121. https://doi.org/10.1029/2011JD016387

Hanna, E., Huybrechts, P., Steffen, K., Cappelen, J., Huff, R., Shuman, C., et al. (2008). Increased runoff from melt from the Greenland Ice Sheet: A response to global warming. *Journal of Climate*, *21*, 331–341. https://doi.org/10.1175/2007JCLI1964.1

Hanna, E., Jones, J. M., Cappelen, J., Mernild, S. H., Wood, L., Steffen, K., & Huybrechts, P. (2013). The influence of North Atlantic atmospheric and oceanic forcing effects on 1900–2010 Greenland summer climate and ice melt/runoff. *International Journal of Climatology*, *33*(4), 862–880. https://doi.org/10.1002/joc.3475

Henley, B. J., Gergis, J., Karoly, D. J., Power, S., Kennedy, J., & Folland, C. K. (2015). A tripole index for the interdecadal Pacific oscillation. *Climate Dynamics*, *45*(11–12), 3077–3090. https://doi.org/10.1007/s00382-015-2525-1

Hofer, D., Raible, C. C., Merz, N., Dehnert, A., & Kuhlemann, J. (2012). Simulated winter circulation types in the North Atlantic and European region for preindustrial and glacial conditions. *Geophysical Research Letters*, *39*, L15805. https://doi.org/10.1029/2012GL052296

Hu, Y., Xia, Y., Liu, Z., Wang, Y., Lu, Z., & Wang, T. (2020). Distorted Pacific–North American teleconnection at the Last Glacial Maximum. *Climate of the Past*, *16*, 199–209. https://doi.org/10.5194/cp-16-199-2020

Hurrell, J. W. (1995). Decadal trends in the North Atlantic Oscillation: Regional temperatures and precipitation. *Science*, *269*(5224), 676 LP–679. https://doi.org/10.1126/science.269.5224.676

Hurrell, J. W., Kushnir, Y., Ottersen, G., & Visbeck, M. (2003). *An Overview of the North Atlantic Oscillation*, *Geophysical Monograph* (Vol. 134, pp. 1–36). Washington, DC: American Geophysical Union.

Justino, F., & Peltier, W. R. (2005). The glacial North Atlantic Oscillation. *Geophysical Research Letters*, *32*, L21803. https://doi.org/10.1029/2005GL023822

Kageyama, M., Albani, S., Braconnot, P., Harrison, S. P., Hopcroft, P. O., Ivanovic, R. F., et al. (2017). The PMIP4 contribution to CMIP6—Part 4: Scientific objectives and experimental design of the PMIP4-CMIP6 Last Glacial Maximum experiments and PMIP4 sensitivity experiments. *Geoscientific Model Development*, *10*(11), 4035–4055. https://doi.org/10.5194/gmd-10-4035-2017

Kageyama, M., D'Andrea, F., Ramstein, G., Valdes, P. J., & Vautard, R. (1999). Weather regimes in past climate atmospheric general circulation model simulations. *Climate Dynamics*, *15*(10), 773–793. https://doi.org/10.1007/s003820050315

Kajtar, J. B., Collins, M., Frankcombe, L. M., England, M. H., Osborn, T. J., & Juniper, M. (2019). Global mean surface temperature response to large-scale patterns of variability in observations and CMIP5. *Geophysical Research Letters*, *46*, 2232–2241. https://doi.org/10.1029/2018GL081462

Kleppin, H., Jochum, M., Otto-Bliesner, B., Shields, C. A., & Yeager, S. (2015). Stochastic atmospheric forcing as a cause of Greenland climate transitions. *Journal of Climate*, *28*(19), 7741–7763. https://doi.org/10.1175/JCLI-D-14-00728.1

Kobashi, T., Box, J. E., Vinther, B. M., Goto-Azuma, K., Blunier, T., White, J. W. C., et al. (2015). Modern solar maximum forced late twentieth century Greenland cooling. *Geophysical Research Letters*, *42*, 5992–5999. https://doi.org/10.1002/2015GL064764

Kushnir, Y., Robinson, W. A., Bladé, I., Hall, N. M., Peng, S., & Sutton, R. (2002). Atmospheric GCM response to extratropical SST anomalies: Synthesis and evaluation. *Journal of Climate*, *15*, 2233–2256. https://doi.org/10.1175/1520-0442(2002)015<2233:AGRTES>2.0.CO;2

Latif, M. (2001). Tropical Pacific/Atlantic Ocean interactions at multi-decadal time scales. *Geophysical Research Letters*, *28*(3), 539–542. https://doi.org/10.1029/2000GL011837

Lemke, P., Ren, J., Alley, R. B., Allison, I., Carrasco, J., Flato, G., et al. (2007). Observations: Changes in snow, ice and frozen ground. In S. Solomon, et al. (Eds.), *Climate Change 2007: The Physical Science Basis. Contribution of Working Group I to the Fourth Assessment Report of the Intergovernmental Panel on Climate Change* (pp. 337–383). Cambridge, UK and New York, NY: Cambridge University Press.

Levine, A. F. Z., McPhaden, M. J., & Frierson, D. M. W. (2017). The impact of the AMO on multidecadal ENSO variability. *Geophysical Research Letters*, *44*, 3877–3886. https://doi.org/10.1002/2017GL072524

Liu, Z. (2012). Dynamics of interdecadal climate variability: A historical perspective. *Journal of Climate*, *25*(6), 1963–1995. https://doi.org/10.1175/2011JCLI3980.1

Madec, G. (2008). NEMO ocean engine. Note du Pole de modélisation 27, Institut Pierre-Simon Laplace (p. 193). Retrieved from http://www.nemo-ocean.eu/content/download/5302/31828/file/NEMO_book.pdf

Masson-Delmotte, V., Jouzel, J., Landais, A., Stievenard, M., Johnsen, S. J., White, J. W., et al. (2005). GRIP deuterium excess reveals rapid and orbital-scale changes in Greenland moisture origin. *Science*, *309*(5731), 118–121. https://doi.org/10.1126/science.1108575

Merkel, U., Prange, M., & Schulz, M. (2010). ENSO variability and teleconnections during glacial climates. *Quaternary Science Reviews*, *29*(1–2), 86–100. https://doi.org/10.1016/J.QUASCIREV.2009.11.006

Newman, M., Alexander, M. A., Ault, T. R., Cobb, K. M., Deser, C., di Lorenzo, E., et al. (2016). The Pacific decadal oscillation, revisited. *Journal of Climate*, *29*(12), 4399–4427. https://doi.org/10.1175/JCLI-D-15-0508.1

Noël, B., Fettweis, X., van de Berg, W. J., van den Broeke, M. R., & Erpicum, M. (2014). Sensitivity of Greenland Ice Sheet surface mass balance to perturbations in sea surface temperature and sea ice cover: A study with the regional climate model MAR. *The Cryosphere*, *8*, 1871–1883. https://doi.org/10.5194/tc-8-1871-2014

Park, W., Keenlyside, N., Latif, M., Ströh, A., Redler, R., Roeckner, E., & Madec, G. (2009). Tropical Pacific climate and its response to global warming in the Kiel Climate Model. *Journal of Climate*, *22*(1), 71–92. https://doi.org/10.1175/2008JCLI2261.1

Parker, D., Folland, C., Scaife, A., Knight, J., Colman, A., Baines, P., & Dong, B. (2007). Decadal to multidecadal variability and the climate change background. *Journal of Geophysical Research*, *112*, D18115. https://doi.org/10.1029/2007JD008411

Pausata, F. S. R., Li, C., Wettstein, J. J., Kageyama, M., & Nisancioglu, K. H. (2011). The key role of topography in altering North Atlantic atmospheric circulation during the last glacial period. *Climate of the Past*, *7*(4), 1089–1101. https://doi.org/10.5194/cp-7-1089-2011

Pausata, F. S. R., Li, C., Wettstein, J. J., Nisancioglu, K. H., & Battisti, D. S. (2009). Changes in atmospheric variability in a glacial climate and the impacts on proxy data: A model intercomparison. *Climate of the Past*, *5*(3), 489–502. https://doi.org/10.5194/cp-5-489-2009

Power, S., Delage, F., Wang, G., Smith, I., & Kociuba, G. (2017). Apparent limitations in the ability of CMIP5 climate models to simulate recent multi-decadal change in surface temperature: Implications for global temperature projections. *Climate Dynamics*, *49*(1–2), 53–69. https://doi.org/10.1007/s00382-016-3326-x

Rahmstrof, S., Crucifix, M., Ganopolski, A., Goosse, H., Kamenkovich, I., Knutti, R., et al. (2005). Thermohaline circulation hysteresis: A model intercomparison. *Geophysical Research Letters*, *32*, L23605. https://doi.org/10.1029/2005GL023655

Rehfeld, K., Münch, T., Ho, S. L., & Laepple, T. (2018). Global patterns of declining temperature variability from the Last Glacial Maximum to the Holocene. *Nature*, *554*(7692), 356–359. https://doi.org/10.1038/nature25454

Rhines, A., & Huybers, P. J. (2014). Sea ice and dynamical controls on preindustrial and last glacial maximum accumulation in central Greenland. *Journal of Climate*, *27*(23), 8902–8917. https://doi.org/10.1175/JCLI-D-14-00075.1

Rimbu, N., Lohmann, G., Werner, M., & Ionita, M. (2017). Links between central Greenland stable isotopes, blocking and extreme climate variability over Europe at decadal to multidecadal time scales. *Climate Dynamics*, *49*(1–2), 649–663. https://doi.org/10.1007/s00382-016-3365-3

Roeckner, E., Bäuml, G., Bonaventura, L., Brokopf, R., Esch, M., Giorgetta, M., et al. (2003). The atmospheric general circulation model ECHAM5. PART I: Model description. *Max-Planck-Institut für Meteorologie*, *349*. Retrieved from. http://pubman.mpdl.mpg.de/pubman/item/escidoc:995269/component/escidoc:995268/Report-349.pdf

Saha, S., Moorthi, S., Pan, H.-L., Wu, X., Wang, J., Nadiga, S., et al. (2010). The NCEP climate forecast system reanalysis. *Bulletin of the American Meteorological Society*, *91*(8), 1015–1058. https://doi.org/10.1175/2010BAMS3001.1

Schulz, J., Dümenil, L., & Polcher, J. (2001). On the land surface–atmosphere coupling and its impact in a single-column atmospheric model. *Journal of Applied Meteorology*, *40*, 642–663. https://doi.org/10.1175/1520-0450(2001)040<0642:OTLSAC>2.0.CO;2

Seierstad, I. A., & Bader, J. (2009). Impact of a projected future Arctic Sea Ice reduction on extratropical storminess and the NAO. *Climate Dynamics*, *33*, 937. https://doi.org/10.1007/s00382-008-0463-x

Shao, Z.-G., & Ditlevsen, P. D. (2016). Contrasting scaling properties of interglacial and glacial climates. *Nature Communications*, *7*, 10951.

Song, Z., Latif, M., & Park, W. (2019). East Atlantic pattern drives multidecadal Atlantic meridional overturning circulation variability during the last glacial maximum. *Geophysical Research Letters*, *46*, 10,865–10,873. https://doi.org/10.1029/2019GL082960

Takaya, K., Nakamura, H., Takaya, K., & Nakamura, H. (2001). A formulation of a phase-independent wave-activity flux for stationary and migratory quasigeostrophic eddies on a zonally varying basic flow. *Journal of the Atmospheric Sciences*, *58*(6), 608–627. https://doi.org/10.1175/1520-0469(2001)058<0608:AFOAPI>2.0.CO;2

Valcke, S. (Ed.) (2006). OASIS3 user guide (PRISM_2–5). CERFACS technical report TR/CMGC/06/73, PRISM Report No 3 (p. 60). Toulouse, France. Retrieved from http://www.prism.enes.org/Publications/Reports/oasis3_UserGuide_T3.pdf

Zhang, Y., Wallace, J. M., & Battisti, D. S. (1997). ENSO-like interdecadal variability: 1900–93. *Journal of Climate*, *10*(5), 1004–1020. https://doi.org/10.1175/1520-0442(1997)010<1004:ELIV>2.0.CO;2